ADVANCES IN ATMOSPHERIC SCIENCES, VOL. 35, AUGUST 2018, 1003–1020

• **Original Paper** •

Effect of Horizontal Resolution on the Representation of the Global Monsoon Annual Cycle in AGCMs

Lixia ZHANG*[1,2], Tianjun ZHOU[1], Nicholas P. KLINGAMAN[3], Peili WU[4], and Malcolm ROBERTS[4]

[1]*LASG, Institute of Atmospheric Physics, Chinese Academy of Sciences, Beijing* 100029*, China*

[2]*Collaborative Innovation Center on Forecast and Evaluation of Meteorological Disasters, Nanjing University of Information Science & Technology, Nanjing* 210044*, China*

[3]*National Centre for Atmospheric Science and Department of Meteorology, University of Reading, Reading* RG6 6BB*, United Kingdom*

[4]*Met Office Hadley Centre, Exeter,* EX1 3PB*, United Kingdom*

(Received 30 October 2017; revised 8 January 2018; accepted 8 February 2018)

ABSTRACT

The sensitivity of the representation of the global monsoon annual cycle to horizontal resolution is compared in three AGCMs: the Met Office Unified Model-Global Atmosphere 3.0; the Meteorological Research Institute AGCM3; and the Global High Resolution AGCM from the Geophysical Fluid Dynamics Laboratory. For each model, we use two horizontal resolution configurations for the period 1998–2008. Increasing resolution consistently improves simulated precipitation and low-level circulation of the annual mean and the first two annual cycle modes, as measured by the pattern correlation coefficient and equitable threat score. Improvements in simulating the summer monsoon onset and withdrawal are region-dependent. No consistent response to resolution is found in simulating summer monsoon retreat. Regionally, increased resolution reduces the positive bias in simulated annual mean precipitation, the two annual-cycle modes over the West African monsoon and Northwestern Pacific monsoon. An overestimation of the solstitial mode and an underestimation of the equinoctial asymmetric mode of the East Asian monsoon are reduced in all high-resolution configurations. Systematic errors exist in lower-resolution models for simulating the onset and withdrawal of the summer monsoon. Higher resolution models consistently improve the early summer monsoon onset over East Asia and West Africa, but substantial differences exist in the responses over the Indian monsoon region, where biases differ across the three low-resolution AGCMs. This study demonstrates the importance of a multi-model comparison when examining the added value of resolution and the importance of model physical parameterizations for simulation of the Indian monsoon.

Key words: global monsoon, high resolution modeling, monsoon annual cycle, AMIP

Citation: Zhang, L. X., T. J. Zhou, N. P. Klingaman, P. Wu, and M. Roberts, 2018: Effect of horizontal resolution on the representation of the global monsoon annual cycle in atmospheric general circulation models. *Adv. Atmos. Sci.*, **35**(8), 1003–1020, https://doi.org/10.1007/s00376-018-7273-9.

1. Introduction

Monsoons are characterized by a seasonal wet–dry contrast and a reversal of prevailing winds, due to the reversal of land–sea and inter-hemispheric thermal contrasts forced by the annual cycle of solar heating. The global monsoon is a dominant mode of annual variability of the global tropical circulation and is a response of the coupled climate system to annual variations in solar forcing (Wang and Ding, 2008). Global monsoon regions sustain nearly two-thirds of the world's population and support some of the largest and fastest-growing urban areas. The simulation and prediction of the annual cycle of monsoon circulation and precipitation is critically important, because of the effect of monsoons on hydrology, agriculture and local livelihoods and economies.

Although global monsoon regions are connected through mass conservation (Trenberth et al., 2000), each regional monsoon has unique characteristics due to the local interactions among the land surface, ocean, convection and synoptic weather systems, especially over the Asian–Australian monsoon region. The well-recognized Asian monsoon system typically first onsets over the Bay of Bengal (BoB) in early May, followed by the South China Sea in mid-May and then India in early June (Wu and Zhang, 1998; Xu and Chan, 2001; Mao and Wu, 2007). The onset over the BoB is often preceded by the development of a monsoon onset vortex (Krishnamurti and Ramanathan, 1982; Wu et al., 2012). A

* Corresponding author: Lixia ZHANG
Email: lixiazhang@mail.iap.ac.cn

numerical study by Liu et al. (2002) demonstrated that the onset of the South China Sea monsoon is due to a Rossby wave train triggered by the strong latent heating during the BoB monsoon onset. The seasonal march of the East Asian summer monsoon (EASM) displays a stepwise northward and northeastward advance. From early May to mid-May, the ridge line of the western Pacific subtropical high (WPSH) is located along 15°N, and southern China experiences a premonsoon rainy season. Later, the WPSH exhibits two northward jumps, in June and July, with the ridge line located at 20°N and 25°N, respectively, the monsoon rain band extends abruptly from the Indochina Peninsula–the South China Sea–the Philippines to the Yangtze River valley in early to mid-June, and the mei-yu (or baiu in Japan and changma in Korea) begins. The monsoon penetrates northern China (34°–41°N) in mid-July, where the monsoon rainy season lasts for one month and ends in early-mid August (Zhou et al., 2009). For the Australian summer monsoon onset in December, there are four major contributing factors, including land–sea thermal contrast, barotropic instability, arrival of the Madden–Julian Oscillation, and intrusion of a midlatitude trough (Hung and Yanai, 2004). The mean onset of the summer monsoon over West Africa is 24 June, which is linked to an abrupt latitudinal shift of the Intertropical Convergence Zone (ITCZ) from a quasi-stationary location at 5°N in May–June to another quasi-stationary location at 10°N in July–August (Sultan and Janicot, 2003). For the American monsoon, the northward rainbelt movement over southwestern North America from mid–late June is associated with the northward progression of the ITCZ (Yu and Wallace, 2000; Higgins and Shi, 2001), while the onset of the South American monsoon is related to the eastward displacement of the South Atlantic subtropical high; it is also affected by intraseasonal variability through low-frequency trough or ridge occurrence over southern Brazil (Raia and Cavalcanti, 2008). The unique features of regional monsoons and their onsets have been used as rigorous metrics for gauging climate model performance.

The complexity of monsoon systems presents great challenges in simulating the climatological seasonal means and annual cycles of the monsoon (Sperber et al., 2013; Zou and Zhou, 2015; Zhou et al., 2017), although substantial efforts have been made to improve model physics and dynamics in the past several decades. Model biases in the simulation of the monsoons limit the fidelity of monsoon predictions and projections (Dong et al., 2016). Sperber et al. (2013) evaluated the performance of 25 coupled climate models from phase 5 of the Coupled Model Intercomparison Project (CMIP5), and 22 models from phase 3 (CMIP3), in simulating the onset and retreat of the Asian summer monsoon. The authors found an overall delayed onset over India in the models, albeit with the CMIP5 models showing improved fidelity relative to CMIP3. The definition of onset and retreat in Sperber et al. (2013) is based on rainfall thresholds; monsoon onset might not occur in models, or may be delayed relative to observations, because of systematic dry biases. To avoid this issue, Sperber and Annamalai (2014) proposed a fractional accumulation method to evaluate the monsoon annual cycle; this method can be applied to many monsoon domains. The authors also found some systematic errors in the phase of the rainfall annual cycle: coupled climate models in CMIP5 have delayed onsets of summer rainfall over India, the Gulf of Guinea, and South America, but early onsets for the Sahel and North America.

Several studies have proposed techniques to improve monsoon simulation, including increasing the horizontal resolution to capture large-scale atmospheric circulations and precipitation distributions more realistically (Hack et al., 2006; Roberts et al., 2009; Berckmans et al., 2013; Demory et al., 2014). The added value of resolution in GCMs has been widely verified for many aspects of monsoon simulation (Kitoh and Kusunoki, 2008; Mizuta et al., 2012; Johnson et al., 2016). For example, an examination of the Community Atmosphere Model, version 5.1 (CAM5), at three resolutions, showed a much better representation of the intensity–frequency structures of precipitation in steep-terrain regions over East Asia (Li et al., 2015). Higher resolution in CAM5 also improves the simulation of the EASM rain belt (Yao et al., 2017). Most investigations of the benefits of increased resolution have based on one model; however, the sensitivity to resolution may differ among models. Ogata et al. (2017) showed that the Meteorological Research Institute AGCM3 (MRI-AGCM3) and the Met Office Unified Model-Global Atmosphere 3.0 (MetUM-GA3) produce less precipitation over the western Pacific with increasing resolution, but their sensitivity of Indian Ocean precipitation to resolution differs. Zhang et al. (2016) compared three AGCMs, each with two resolution configurations, and showed the sensitivity of monsoon precipitation to resolution varied greatly among the models. To understand what aspects of resolution sensitivity are common among AGCMs, it is important to compare several AGCMs using the same metrics. Given the social and scientific importance of the onset and cessation of monsoon precipitation to local livelihoods and economies, it is desirable to find out whether high resolution systematically improves the representation of monsoon onset and withdrawal. This is the major motivation behind the current study.

The remainder of the paper is organized as follows: The model simulations, validation data and evaluation metrics are described in section 2. The improvements in simulating the annual cycle modes and monsoon onset and withdrawal by increasing the resolution are assessed in sections 3 and 4, respectively. Section 5 presents a summary and discussion.

2. Models, data and methods

2.1. *Model simulations and observational validation datasets*

We use daily precipitation and monthly wind data from simulations with three AGCMs—MetUM-GA3, MRI-AGCM3 and the Global High Resolution AGCM from the Geophysical Fluid Dynamics Laboratory (GFDL-HiRAM)—each with two resolution configurations, for the period 1998–

2008. Details of the models and experiments can be found in Table 1. The model outputs of GFDL-HiRAM and MRI-AGCM3 are from the CMIP5 (Taylor et al., 2012) data archive. The simulations of MetUM-GA3 are from the UPSCALE (UK on PRACE Weather-resolving Simulations of Climate for Global Environmental Risk) project (Mizielinski et al., 2014). There are very few different physical and dynamical settings in the MetUM-GA3 high-resolution configuration compared to its low-resolution counterparts, mostly related to numerical stability (Table 2 in Mizielinski et al., 2014). There are no physical parameter adjustments between the high-resolution (MRI-AGCM3-2H) and super-high resolution (MRI-AGCM3.2S) versions (Endo et al., 2012; Kusunoki, 2016). In GFDL-HiRAM, the shallow convective scheme and cloud microphysics are changed to C360 from C180 (Zhao et al., 2009; Chen and Lin, 2013). We analyze the ensemble mean of all realizations of each model. Because of the large inter-model differences in dynamical cores and physics, it is hard to compare the resolution sensitivity across models. To exclude the impact of model-dependence and focus more on resolution, we compare the high- and low-resolution configurations of each model in this study.

The observed daily precipitation datasets used in this study include: (1) the Tropical Rainfall Measuring Mission (TRMM) 3B42 V7 product (Huffman et al., 2007), to evaluate the climatological mean state of global monsoon precipitation, at $0.25^\circ \times 0.25^\circ$ resolution; and (2) version 1.2 of the Global Precipitation Climatology Project (GPCP), with a resolution $1.0^\circ \times 1.0^\circ$ (Adler et al., 2003). In addition, monthly wind data from the Climate Forecast System Reanalysis (CFSR; Saha et al., 2009), with a resolution of $0.5^\circ \times 0.5^\circ$, and from the National Centers for Environmental Prediction–National Center for Atmospheric Research (NCEP–NCAR) reanalysis, with a resolution $2.5^\circ \times 2.5^\circ$ (Kalnay et al., 1996), are used as the circulation datasets. All datasets are interpolated to the N216 resolution of MetUM-GA3 (approximately 0.83° longitude $\times 0.55^\circ$ latitude) using a distance-weighted interpolation method, to facilitate comparison. The longest common period of 1998–2008 covered by all simulations and observations is selected in the following analysis.

2.2. *Evaluation metrics on global monsoon annual cycles*

In this study, two aspects of the annual cycle of the global monsoon are evaluated: (1) the mean climate and annual cycle modes; and (2) monsoon onset and withdrawal. As proposed by Wang and Ding (2008), the annual mean, the solstitial (symmetric) and equinoctial (asymmetric) modes of the annual cycle, and the global monsoon domain can be used as metrics to gauge model performance for simulating the mean climate and annual cycle. The solstitial mode is represented by the differences in precipitation or circulation between the June–September and December–March means; the equinoctial asymmetric mode is represented by the differences between April–May and October–November. The global monsoon domain is delineated both by the monsoon precipitation index (MPI) and monsoon wind index (MWI). The MPI is defined as the annual range of precipitation normalized by its annual mean; the MWI is similar, but using 850-hPa zonal wind (U850). The monsoon precipitation domains are the areas where the annual range of precipitation exceeds 300 mm and the MPI exceeds 0.5; whereas, the monsoon wind domains are defined as the WMI exceeding 0.5, without any restriction on the magnitude of annual range. The annual range is the difference between the May–September (MJJAS) and November–March (NDJFM) means in the Northern Hemisphere (NH), or NDJFM minus MJJAS in the Southern Hemisphere (SH).

Previous studies have proposed several definitions of

Table 1. Model information, including resolution, sea surface temperature (SST) forcing, realization numbers, and selected simulation years.

Model	Resolution (lat × lon)	SST	Realizations	Selected years
MetUM-GA3	N216 ($0.83^\circ \times 0.55^\circ$)	OSTIA (Donlon et al., 2012)	3	1998–2008
	N512 ($0.35^\circ \times 0.23^\circ$)	OSTIA (Donlon et al., 2012)	5	1998–2008
GFDL-HiRAM	C180 ($0.625^\circ \times 0.5^\circ$)	HadISST1 (Rayner et al., 2003)	3	1998–2008
	C360 ($0.31^\circ \times 0.25^\circ$)	HadISST1 (Rayner et al., 2003)	2	1998–2008
MRI-AGCM3	2H ($0.56^\circ \times 0.56^\circ$)	HadISST1 (Rayner et al., 2003)	2	1998–2008
	2S ($0.18^\circ \times 0.18^\circ$)	HadISST1 (Rayner et al., 2003)	1	1998–2008

Table 2. Schematic contingency table for computing the ETS metric for model simulations of the monsoon domain modified from Jolliffe and Stephenson 2003.

		Event observed		
		Monsoon domain	Non-monsoon domain	Total
Simulation	Monsoon domain	a (hits)	b (false alarms)	$a+b$
	Non-monsoon domain	c (misses)	d (correct rejections)	$c+d$
	Total	$a+c$	$b+d$	$a+b+c+d=n$

monsoon onset and withdrawal. The commonly used definition is threshold-based (Wang and LinHo, 2002). One of the weaknesses of the threshold-based techniques is that monsoon onset might be delayed or accelerated by dry or wet biases, respectively, in the model, even though the model may have a realistic annual cycle amplitude (Sperber et al., 2013; Sperber and Annamalai, 2014). Models with dry biases are especially at a disadvantage since the observed threshold for defining monsoon may never be reached in such models, including MetUM-GA3 in this study (Johnson et al., 2016). Since the biases differ among the three models used here, it is important to find a relatively fair way to evaluate model onset and withdrawal. Thus, a fractional accumulation approach is employed here. The monsoon onset and withdrawal are defined as the pentad when the fractional accumulation first becomes $\geqslant 0.2$ and $\geqslant 0.8$, respectively (Sperber and Annamalai, 2014). The fractional accumulated precipitation in a given pentad is the accumulated rainfall in that pentad divided by the total accumulated rainfall at the end of the year. In this study, the pentads for the southern Africa, Australia and South America domains are reordered to run from 2 July to 27 June.

To quantitatively show the sensitivity of the simulated monsoon domain to resolution, the equitable threat score (ETS; Jolliffe and Stephenson, 2003) is used in this study to measure the simulation skill of the monsoon domain, which can be evaluated as a binary event:

$$\mathrm{ETS} = (a - \mathrm{ar})/(a + b + c - \mathrm{ar}) , \qquad (1)$$

where $\mathrm{ar} = (a + b)(a + c)/n$ represents the skill of a random prediction, in which a, b and c are the hit, false alarm and miss counts of a gridpoint in a monsoon domain, respectively, and n is the number of model gridpoints in the region (45°S–45°N). The definition of each variable in equation (1) can be found in Table 2. ETS ranges from 0 to 1 with perfect score of 1.

3. Annual mean and annual cycle modes

To investigate the consistent improvement from higher resolution across the three models, we analyze the biases in the lower-resolution configuration and the differences between the high- and low-resolution configurations. The bias in simulated annual mean precipitation and improvements from higher resolution are presented in Fig. 1. In observations (blue lines in left-hand panels of Fig. 1), substantial precipitation falls in the Indo-Pacific warm pool (60°E–180°), ITCZ and South Pacific Convergence Zone (SPCZ). In general, the observed centers are captured well by the low-resolution configuration of each AGCM, with an overall positive bias over most of the tropics (blue lines in right-hand panels of Fig. 1). In contrast, there are several common biases among the three low-resolution AGCMs, including overestimations over the southwest Indian Ocean, SPCZ, northern edge of the ITCZ, and the northwestern Pacific Ocean, with underestimations over the southeastern Indian Ocean (Figs. 1a, c and e). Unique biases in each AGCM are also found, particularly in MetUM-GA3 N216, which underestimates Indian and Maritime Continent (MC) precipitation (Fig. 1a). A positive bias over the western central Pacific (5°S–5°N, 120°E–180°) is seen in MRI-AGCM3-2H, while negative biases are present in MetUM-GA3 N216 and GFDL-HiRAM-C180. A consistent response to higher resolution among the three models is suppressed precipitation over the northern MC and western Pacific (5°S–15°N, 120°–160°E), which partly reduces the wet bias over the northwestern Pacific (5°–15°N, 120°–160°E) in the three low-resolution models. This consistent response to finer resolution has also been illustrated by Ogata et al. (2017), who compared MetUM-GA3 and MRI-AGCM3. This is further verified with one additional model, GFDL-HiRAM. As suggested by Ogata et al. (2017) and Johnson et al. (2016), the reduced precipitation over the northern MC and western Pacific may be related to better-resolved steep topography over the MC and Indochina, with moisture convergence and precipitation on the windward side of the orography, which leads to decreased moisture availability on the leeward side in summer and reduced precipitation over the northern MC and western Pacific. This can be partly seen from the difference between higher- and lower-resolution models in simulating the solstitial mode in Fig. 2. Note that the low-resolution versions of both MetUM-GA3 and GFDL-HiRAM underestimate the precipitation over the MC, and the consistent response to resolution makes this dry bias even worse.

As in Fig. 1, the biases in low-resolution models and improvement in higher-resolution configurations for the solstitial mode are shown in Fig. 2. The observed spatial pattern shows an asymmetric contrast, with positive centers in NH monsoon regions [Indian Ocean–Pacific Ocean–East Asia, West Africa and northeastern tropical Pacific (5°–20°N, 120°–60°W)] and negative centers in Southern Hemisphere monsoon regions (South Africa, Australia and South America; lines in left-hand panels of Fig. 2). The centers are reproduced well by all the low-resolution models, but all show underestimations over East Asia, the northeastern tropical Pacific, South Africa and Australia regions, and overestimations over the northwestern Pacific (shading in left-hand panels of Fig. 2). Higher resolution reduces this consistent simulation bias, particularly over the northwestern Pacific and northeastern tropical Pacific (shading in left-hand panels of Fig. 2). The improvement, however, is far smaller than the low-resolution model bias. The biases in the three low-resolution models differ greatly over the Indian monsoon region, where the solstitial mode is dramatically smaller than observation in MetUM-GA3 N216, greater in MRI-AGCM3.2H, and close to observation in GFDL-HiRAM-C180. The sensitivity of the solstitial mode in each model to resolution also differs over the Indian monsoon region. The inconsistency of model biases and sensitivity to resolution indicate the strong role played by subgrid-scale physical parameterizations in simulating the Indian monsoon precipitation.

The biases in the simulated equinoctial asymmetric mode of the annual cycle and corresponding improvements in high-

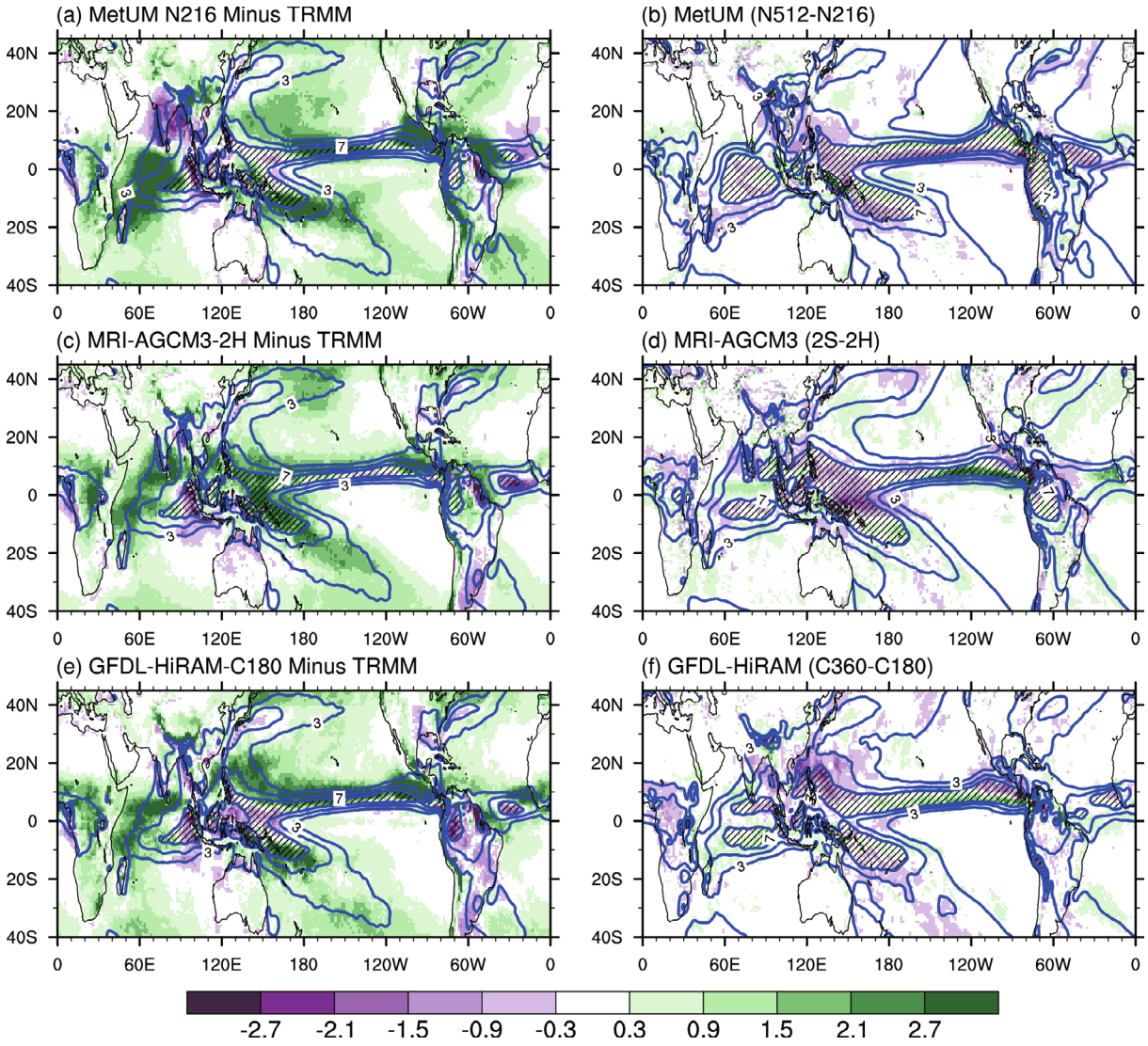

Fig. 1. Spatial distributions of the difference between low-resolution models and TRMM (left-hand column; units: mm d^{-1}) and between high and low resolutions of the same model (right-hand column; units: mm d^{-1}) in simulating annual mean precipitation: (a) MetUM-GA3 N216 minus TRMM; (b) MetUM-GA3 N512 minus MetUM-GA3 N216; (c) MRI-AGCM3-2H minus TRMM; (d) MRI-AGCM3-2S minus MRI-AGCM3-2H; (e) GFDL-HiRAM-C180 minus TRMM; (f) GFDL-HiRAM-C360 minus GFDL-HiRAM-C180. Blue lines in the left- and right-hand columns show the climatological mean precipitation from TRMM and the low-resolution models, respectively. The hatched area denotes where precipitation exceeds 7 mm d^{-1}.

resolution models are shown in Fig. 3. In observations, negative values are centered in the zonal belt along 10°–20°N, while positive values are centered to its south (0°–10°N) and in Southeast China. The centers over the Pacific represent the asymmetric location of the spring and fall ITCZ (Wang and Ding, 2008). The positive values over Southeast China shows the region's characteristic spring-persistence season in April and May (Li et al., 2017). All low-resolution models capture the asymmetric pattern of spring and fall precipitation, but a systematic overestimation over the NH is seen in all models, with negative biases north of the observed negative center and positive biases near the observed positive centers. Positive biases over West Africa are found in all low-resolution models. In high-resolution models, the overestimation over the northwestern Pacific, West Africa and Southeast China is suppressed in all models; consistent improvements are also found over the southern MC. This indicates increased resolution improves simulated precipitation in transition seasons.

To quantify the improvement in high-resolution models, the pattern correlation coefficient (PCC) and root-mean-square error (RMSE) of simulated precipitation over 45°S–45°N against TRMM are shown in Figs. 4a, d and g. The simulated 850-hPa winds for the annual mean and first annual cycle modes against CFSR reanalysis data are also presented in Fig. 4. We compare the metrics for GPCP against TRMM and for NCEP–NCAR against CFSR to show the observational uncertainty. In general, all low-resolution models simulate the observed precipitation and 850-hPa wind patterns

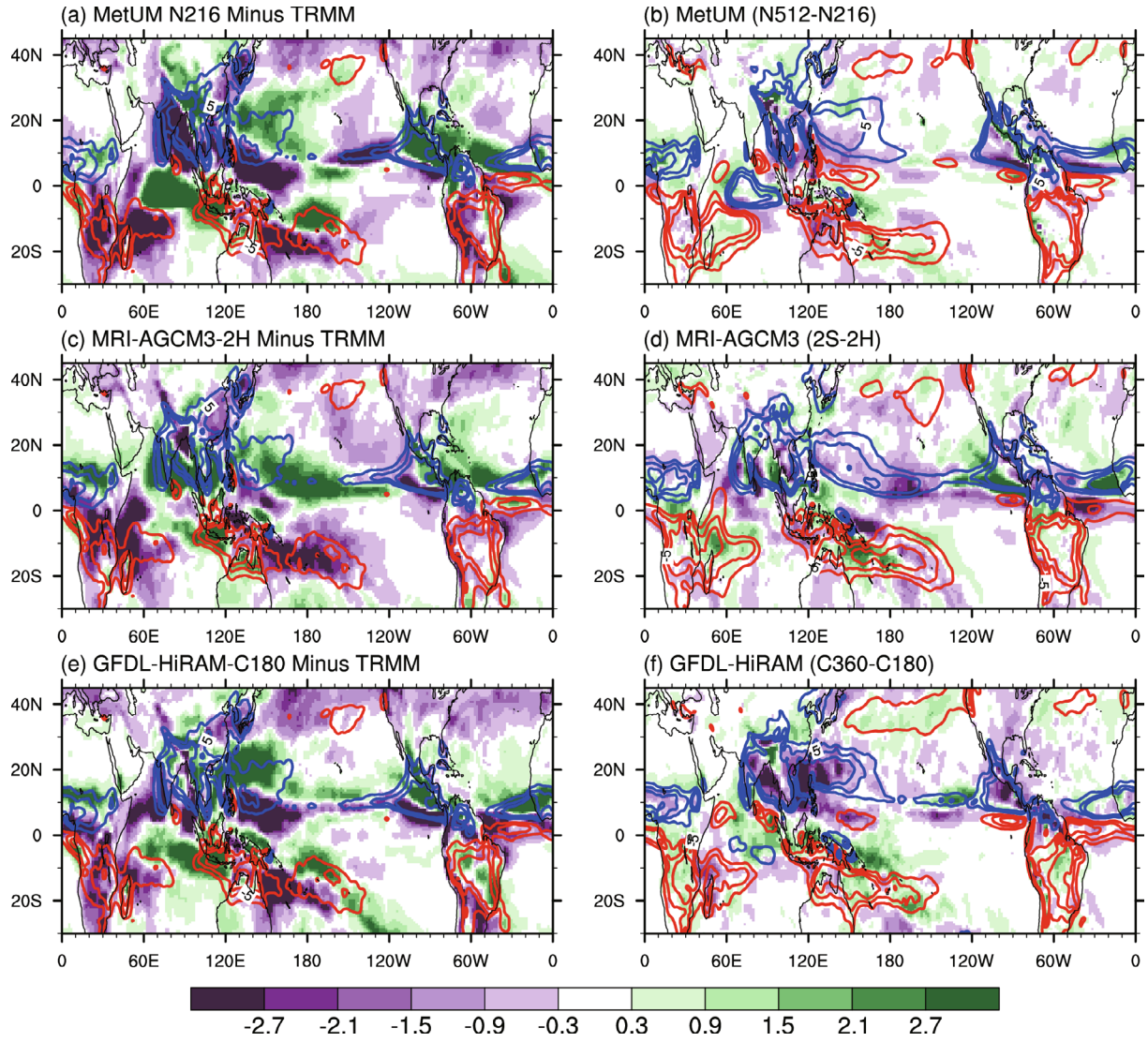

Fig. 2. As in Fig. 1 but for the spatial distribution of the solstitial mode (units: mm d^{-1}), defined as the difference between the June–September and December–March mean precipitation. The blue and red lines indicate positive and negative values, respectively.

well. For example, the PCCs (RMSEs) of simulated annual mean precipitation and 850-hPa zonal (U850) and meridional (V850) wind in the low-resolution models (blue markers in Figs. 4a–c) range from 0.85–0.90 (1.2–1.6 mm d^{-1}), 0.97–0.99 (0.75–1.2 m s^{-1}) and 0.88–0.94 (0.47–0.60 m s^{-1}), respectively, which are close to the PCCs for GPCP and NCEP–NCAR against TRMM and CFSR, respectively. The PCCs increase consistently in all three high-resolution models (red markers) compared with their low-resolution counterparts (blue markers) for the three annual-cycle metrics. However, the model bias, as demonstrated by RMSE, appears insensitive to increasing resolution. The PCCs of annual precipitation, U850 and V850 simulated by the high-resolution models are systematically shifted to the right of the low-resolution ones, increasing to 0.95–0.97, nearly 1.0, and 0.96–0.98, respectively. The PCCs in the high-resolution models are even higher than those of GPCP/NCEP–NCAR, although the RMSEs in these simulations are far larger than in the reanalysis data. The same results are also found in the first two leading modes. High resolution aids in representing the details of precipitation and circulation distributions, but not in reducing model biases.

Following the global monsoon domain definition proposed by Wang and Ding (2008), the distributions of precipitation annual range and monsoon domain based on precipitation are obtained and shown in Fig. 5. In TRMM, the monsoon systems are depicted well by this definition, including the Asian–Australian monsoon, the North and South African monsoons, and the North and South American monsoons (Fig. 5a). The domain obtained from GPCP is similar to that from TRMM, except at the edges, particularly over the northern edge of the northwestern Pacific monsoon region and the southern edge of the southwestern Indian Ocean monsoon region, where the domain areas are relatively larger

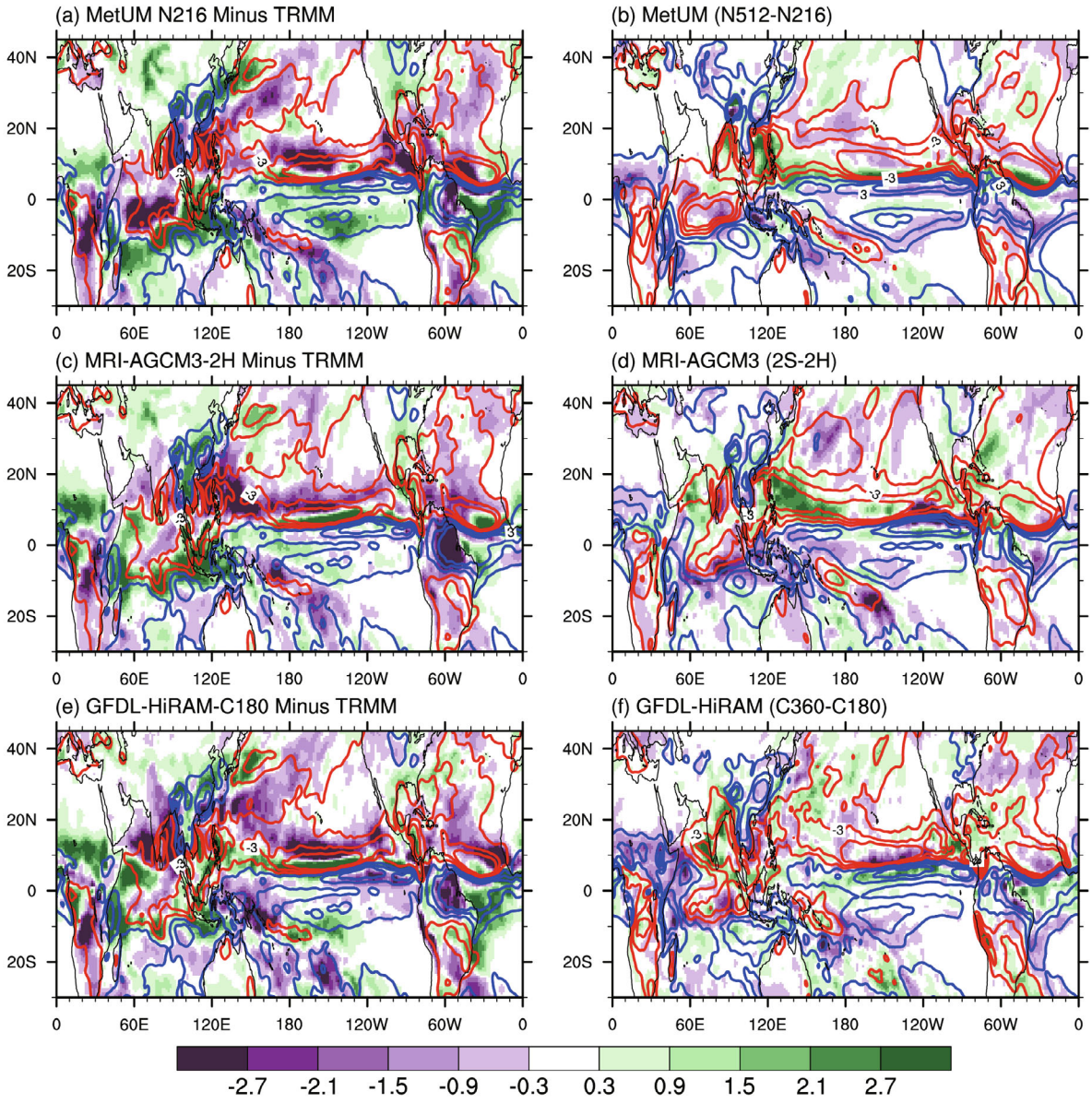

Fig. 3. As in Fig. 1 but for the equinoctial asymmetric mode (units: mm d^{-1}) defined as the difference between the April–May and October–November mean precipitation.

in GPCP than in TRMM. The North American monsoon region (120°–60°W, 0°–20°N) in all low-resolution models is smaller and the western boundary is shifted about 30° eastward relative to observations, while the simulated northwestern Pacific monsoon is wider and stronger than observed (left-hand column in Fig. 5). With increased resolution, the northwestern Pacific monsoon region shrinks relative to the low-resolution models, particularly for MRI-AGCM3, which extends to 170°W in MRI-AGCM3.2H but only to 170°E in MRI-AGCM3.2S. Each model has unique biases, such as the absence of the Indian monsoon region in MetUM-GA3 N216 due to its dry bias in India, a westward extended West African monsoon (60°W–60°E, 0°–20°N) in MetUM-GA3 N216 and MRI-AGCM3.2H due to a wider and stronger ITCZ over the Atlantic Ocean, and an unrealistic monsoon region over the southern tropical Atlantic Ocean in MRI-AGCM3.2H and GFDL-HiRAM-C180. Those biases remain in their high-resolution counterparts, indicating little influence of increased resolution. Similar analysis of the global monsoon domain based on U850 revealed no obvious improvements from increased resolution (data not shown).

To quantitatively show the sensitivity of the simulated monsoon domain to resolution, the ETS (Jolliffe and Stephenson, 2003) for global and individual regional monsoon domains is computed, using precipitation and U850 (Fig. 6). Generally, the higher-resolution configurations show a slightly increased ETS for global monsoon precipitation (wind): from 0.53 to 0.54 (0.63 to 0.67) in MetUM-GA3; 0.56 to 0.57 (0.68 to 0.69) in GFDL-HiRAM; and 0.58 to 0.62 (0.73 to 0.77) in MRI-AGCM3. The ETSs of the three high-

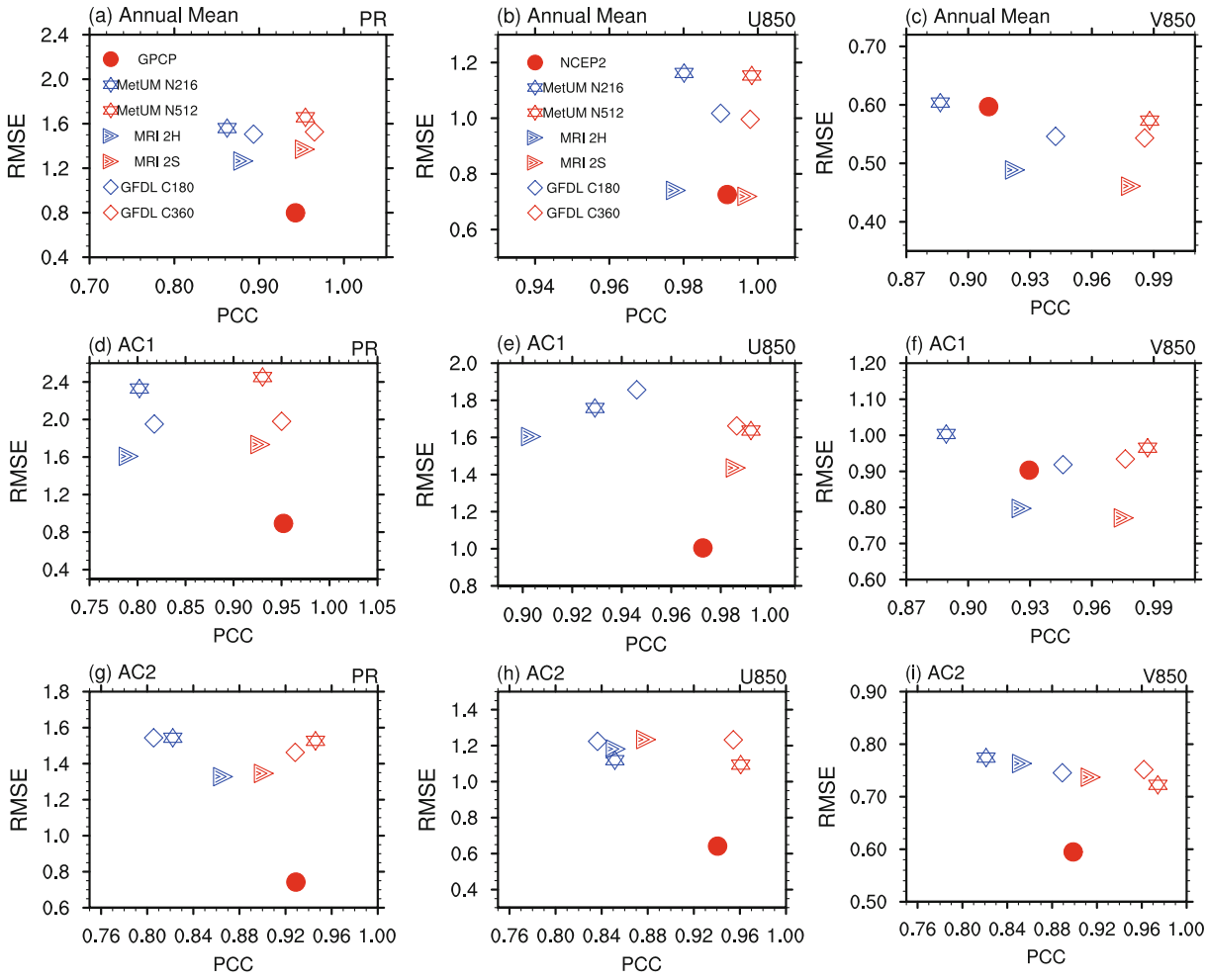

Fig. 4. Scatter plots for the fidelity of simulated precipitation and 850-hPa winds of the (a–c) annual mean, (d–f) solstitial mode, and (g–i) equinoctial asymmetric mode, against TRMM and CFSR. The abscissa and ordinate are the PCC and RMSE (units: mm d^{-1} for precipitation, m s^{-1} for wind), respectively. The fidelity of GPCP (left penal) against TRMM and NCEP–NCAR against CFSR (middle and right panels) are also shown (dots) to represent the observational uncertainty. The stars, triangles and diamonds represent the results from MetUM-GA3, MRI-AGCM3 and GFDL-HiRAM, respectively, with high-resolution configurations in red and low-resolution configurations in blue.

resolution models for regional monsoon precipitation domains are not always higher than their low-resolution counterparts. Consistent improvements with resolution are shown only for the South African monsoon domain, with the largest increase from 0.59 to 0. 64 in MetUM-GA3. The ETSs for regional monsoon wind domains are all higher in the high-resolution configurations. Note that the ETS metrics of U850 and precipitation are not correlated. The skill scores of U850 are higher than those of precipitation for both global and regional monsoons. Even though the higher-resolution models show increased ETSs for U850 for all regional monsoons except the East Asian monsoon, the ETS metrics for precipitation do not increase (e.g., for the Indian monsoon).

4. Monsoon onset and withdrawal

Cumulative rainfall, which is the sum of rainfall up to a given pentad, averaged over each monsoon region is presented in Fig. 7 to show the temporal characteristics of the rainfall and the model bias. A rapid increase in cumulative rainfall occurs in all monsoon regions. However, the initial pentad for the rapid increase differs among regions, indicating different onset times in each region. For the Asian–Australian monsoon system, rapid precipitation increase starts around pentad 30 in India, pentad 25 in Southeast Asia and East Asia, and pentad 10 in Australia. Over the African and American monsoon systems, an onset is observed in pentad 30 in West Africa and North America, and pentad 5 in South Africa and South America.

An overall overestimation of annual total precipitation is presented over all regional monsoons except for India and Southeast Asia. For the Indian monsoon, there is a large disparity among the models in simulated total rainfall. There is an obvious wet bias (50% wetter than TRMM) in MRI-AGCM3, a dry bias (50% less than TRMM) in MetUM-GA3, and a relatively small bias in GFDL-HiRAM (Fig. 7a). The

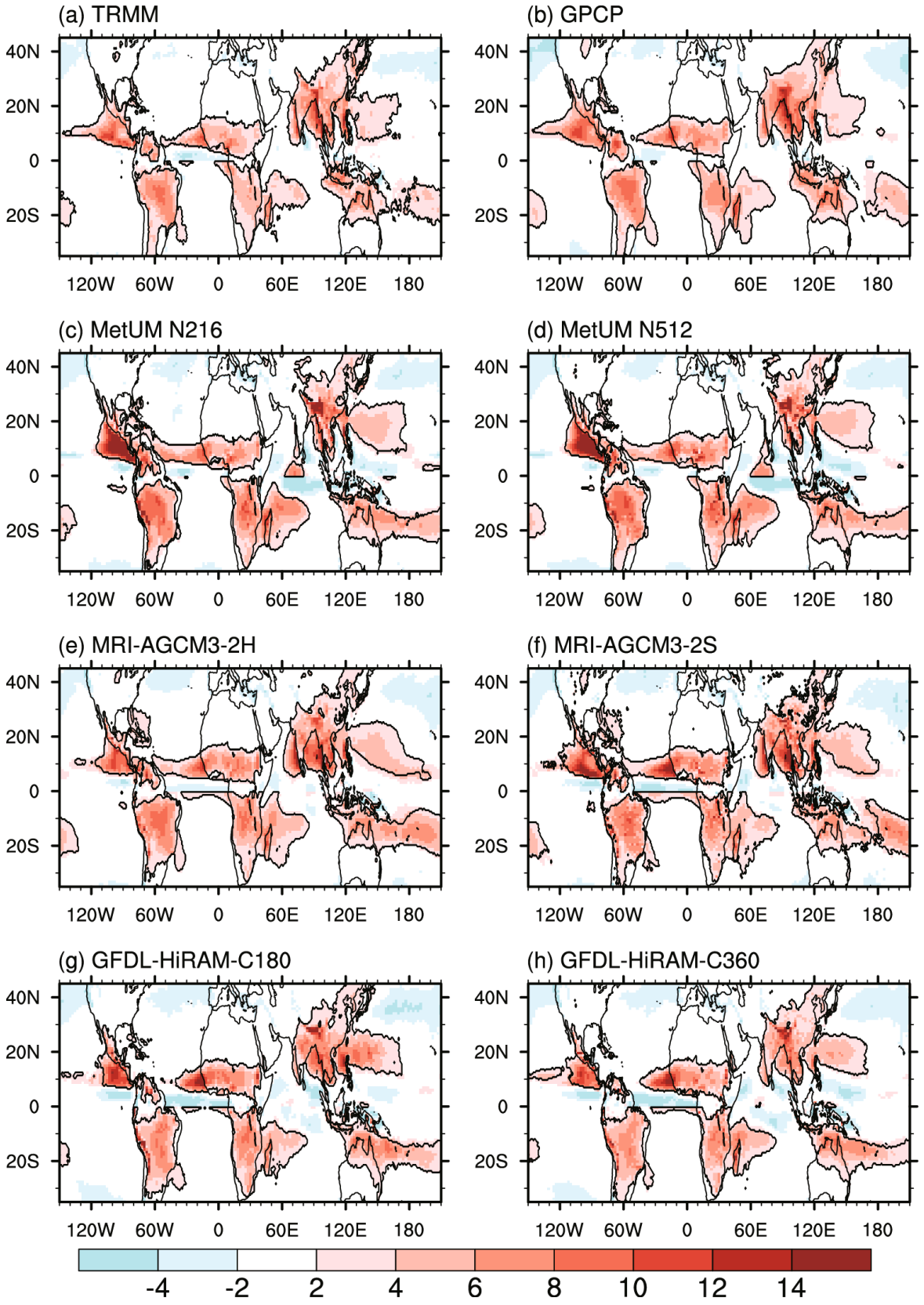

Fig. 5. Climatological annual range of precipitation (shaded; units: mm d^{-1}) and the global monsoon domain (contours) derived from (a) TRMM, (b) GPCP, (c) MetUM-GA3 N216, (d) MetUM-GA3 N512, (e) MRI-AGCM3-2H, (f) MRI-AGCM3-2S, (g) GFDL-HiRAM-C180, and (h) GFDL-HiRAM-C360. The annual range is defined for the NH as the MJJAS minus NDJFM mean precipitation, and for the SH as NDJFM minus MJJAS.

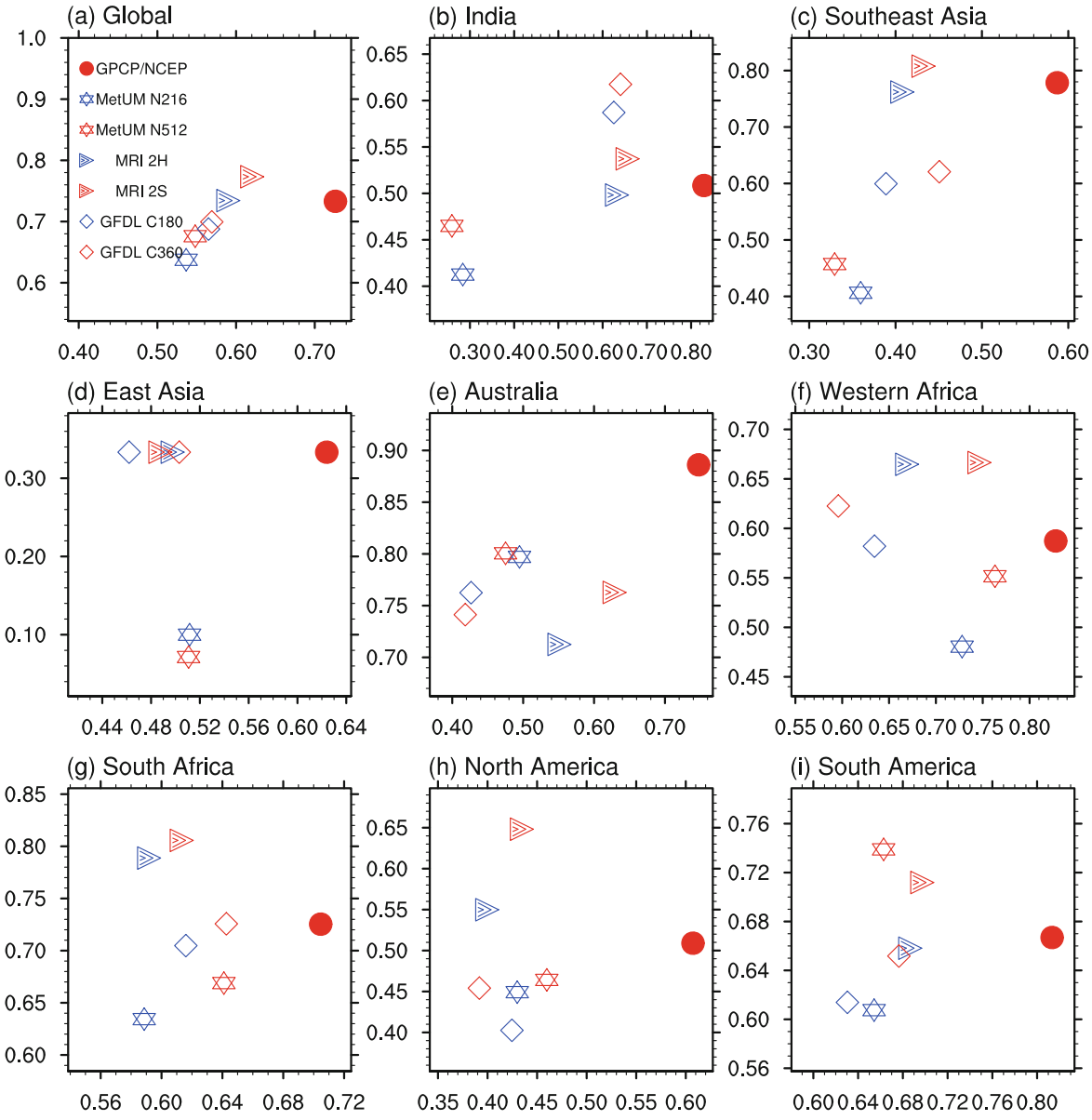

Fig. 6. ETSs of the monsoon domain simulation over the (a) global, (b) Indian, (c) Southeast Asian, (d) East Asian, (e) Australian, (f) West African, (g) South African, (h) North American, and (i) South American monsoons. The abscissa (ordinate) is the ETSs of the simulated domain derived from precipitation (U850). The fidelity of GPCP against TRMM is shown by dots. The fidelity of GPCP and NCEP–NCAR against TRMM and CFSR are also shown by dots, to represent the observational uncertainty. The stars, triangles and diamonds represent the results from MetUM-GA3, MRI-AGCM3 and GFDL-HiRAM, respectively, with high-resolution configurations in red and low-resolution configurations in blue.

biases over Southeast Asia are similar to those over India, but with smaller magnitudes (Fig. 7b). The evolution of cumulative rainfall shows that the bias is relatively small at the beginning of the year, but starts to increase around the monsoon onset pentad.

The observed and simulated spatial distributions of monsoon onset are shown in Fig. 8. The monsoon onset is the pentad when fractional accumulation first becomes $\geqslant 0.2$ (Sperber and Annamalai, 2014). We also examine the distributions of monsoon onset defined by Wang and LinHo (2002), in which onset is determined as the first pentad when the rainfall rate relative to the January mean in the NH, and July in the SH, exceeds 5 mm d^{-1}. This threshold is never reached in MetUM-GA3 over India because of the systematic dry bias (Figs. 1, 2 and 7a). However, India is defined as a monsoon region in MetUM-GA3, based on the monsoon wind index (data not shown). Thus, it is reasonable to use the fractional accumulation to define monsoon onset and withdrawal. To focus on monsoon regions, only the distributions in the observed monsoon regions based on the MPI are shown here. In observations (Figs. 8a and b), the onset pentad shows a gradual increase poleward from the equator, indicating later onset

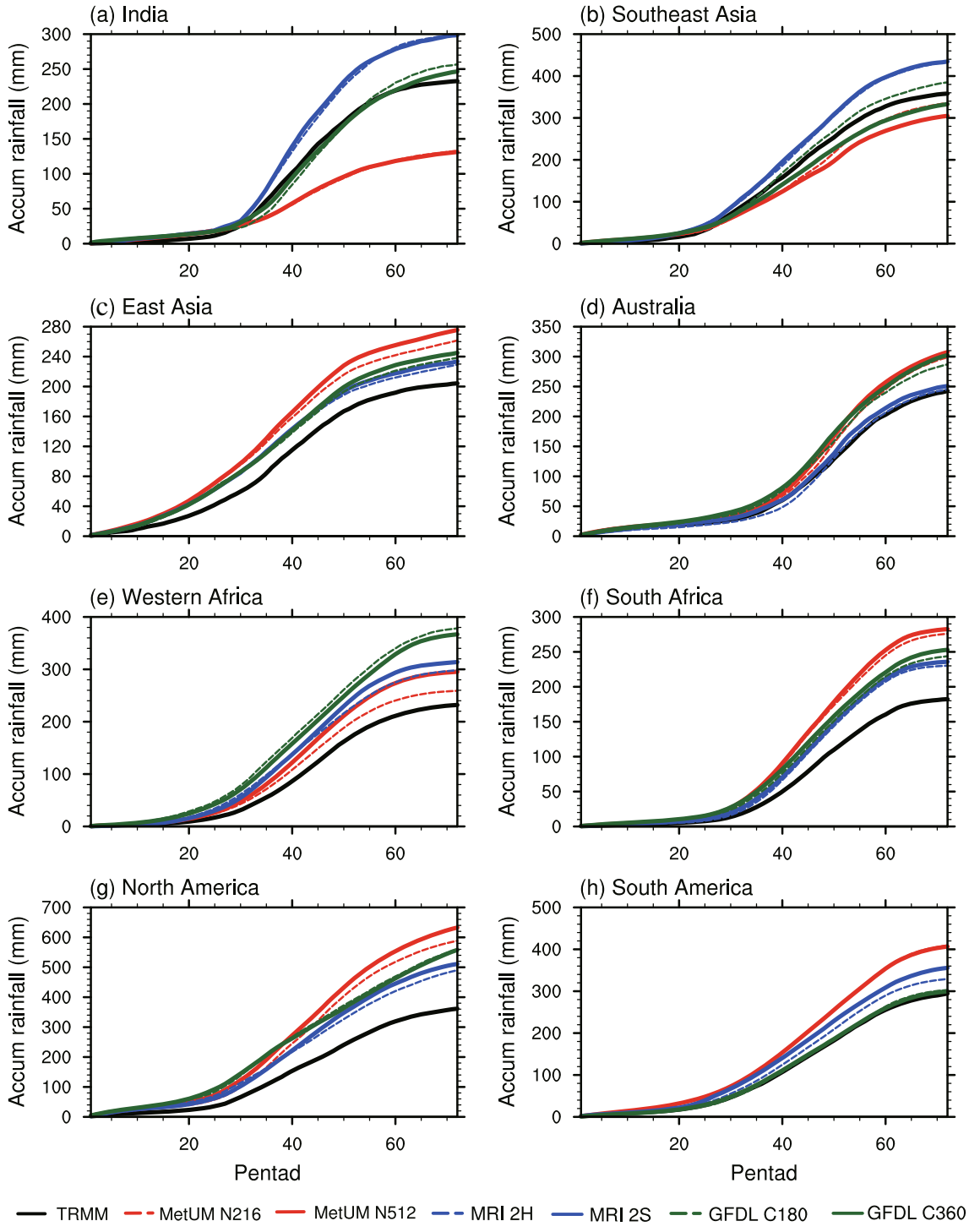

Fig. 7. Observed and simulated cumulative rainfall (units: mm) from the first pentad to the end of year averaged over the (a) Indian, (b) Southeast Asian, (c) East Asian, (d) Australian, (e) West African, (f) South African, (g) North American, and (h) South American monsoons. Note: for the SH locations (Australian, South African, and South American monsoons), the pentads were reordered to July–June prior to the analysis. The black, red, blue and green lines represent the results of TRMM, MetUM-GA3, MRI-AGCM3 and GFDL-HiRAM, respectively, with high-resolution configurations as solid lines and low-resolution configurations as dashed lines.

in the higher-latitude monsoon regions in both hemispheres. In the NH, the earliest onset is pentad 25 in early May over the southern edge of the Northern Hemisphere monsoon region and South China; whereas, in the SH, the earliest onset is pentad 68 in early December over the northern edge of the southwestern Indian Ocean. The latest NH monsoon onset

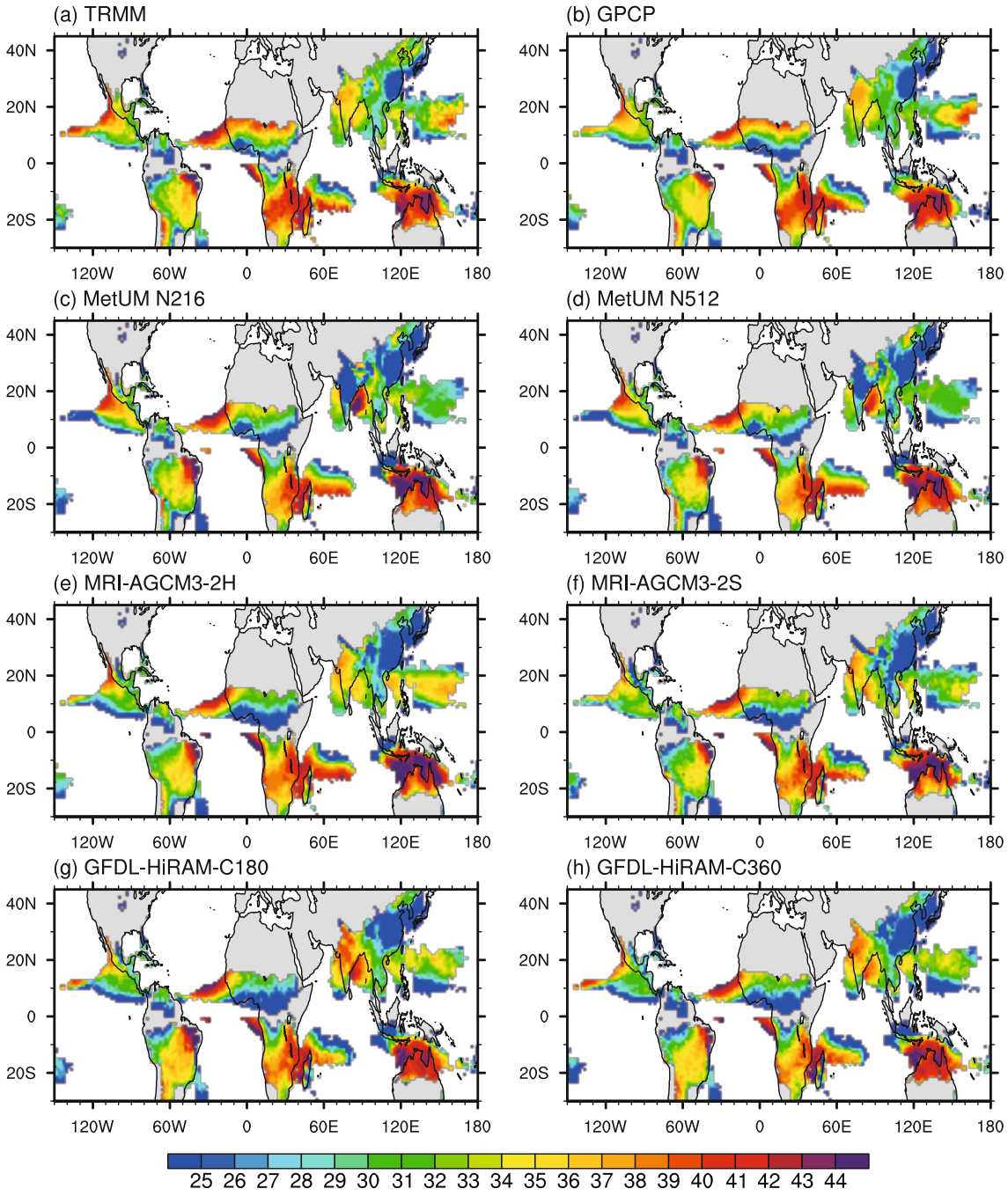

Fig. 8. Climatological monsoon onset pentad derived from (a) TRMM, (b) GPCP, (c) MetUM-GA3 N216, (d) MetUM-GA3 N512, (e) MRI-AGCM3-2H, (f) MRI-AGCM3-2S, (g) GFDL-HiRAM-C180, and (h) GFDL-HiRAM-C360. The monsoon onset pentad is defined as the pentad when fractional accumulation first becomes $\geqslant 0.2$ (Sperber and Annamalai, 2014). Note: for SH locations (Australian, South African, and South American monsoons), the pentads were reordered to July–June prior to the analysis.

is in pentad 47 in mid-August over the northern edge of the North American and West African monsoons (pentad 15 in mid-March over the southern edge of the Australian monsoon in the SH).

All models simulate the spatial distribution of global summer monsoon onset well. However, all the low-resolution models simulate earlier monsoon onsets than the two observed datasets, such as over the East Asian, West African, North American and South American monsoons. Specifically, the area with onset by pentad 25 (hereafter, P25 area) over the West African, North American and East Asian monsoons, is broader than in the observation. In the high-resolution models, the P25 area shrinks slightly over the East Asian and Western African monsoons, particularly apparent in MetUM-GA3. This difference is also seen in the observations, in which the P25 area in GPCP is larger than in TRMM,

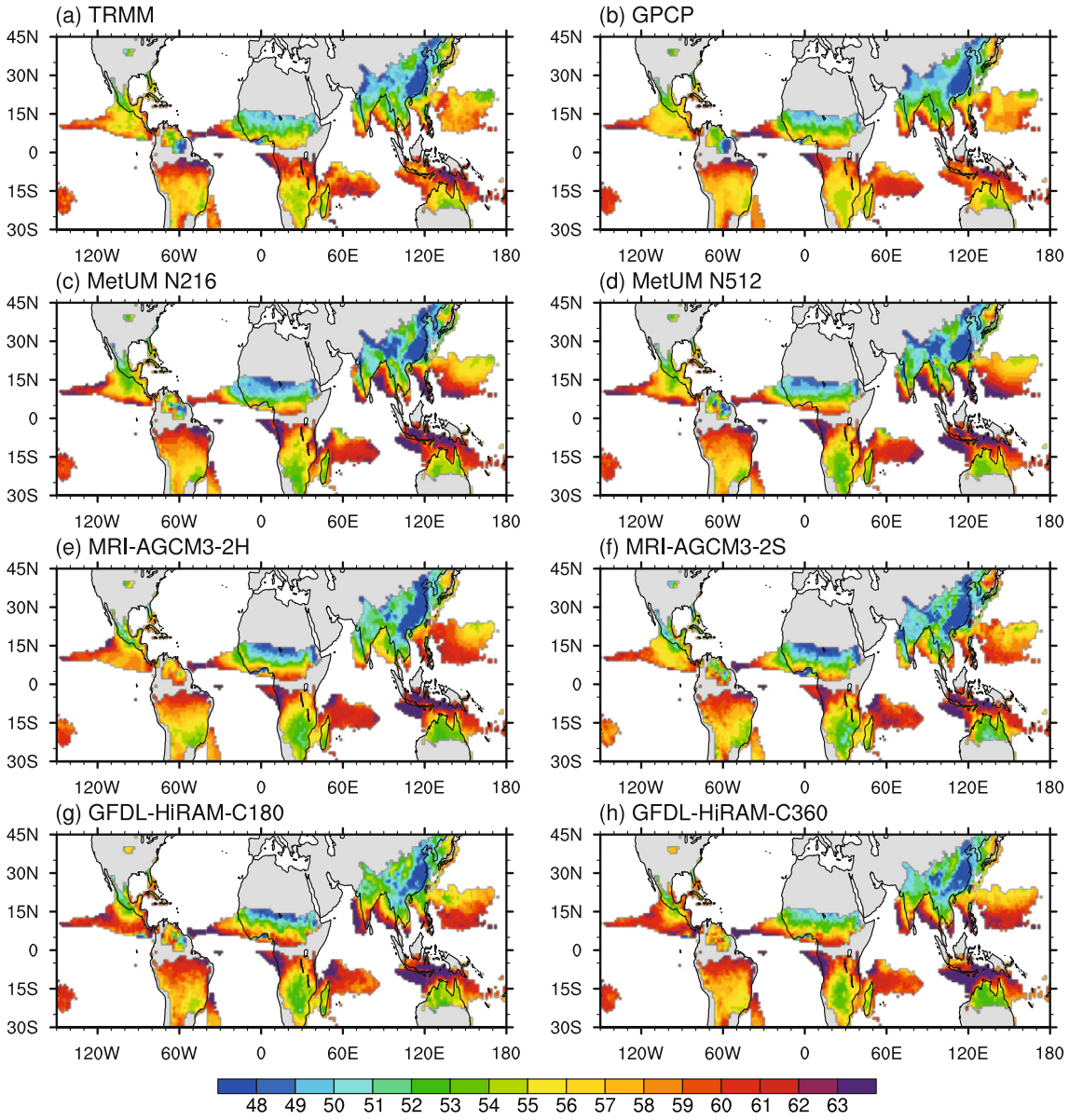

Fig. 9. As in Fig. 8 but for the monsoon withdrawal pentad, defined as the pentad when fractional accumulation first becomes $\geqslant 0.8$ (Sperber and Annamalai, 2014). Note: for SH locations (Australian, South African, and South American monsoons), the pentads were reordered to July–June prior to the analysis.

potentially due to the different resolutions of the two observed datasets. This indicates that high resolution improves the spatial distribution of precipitation and the delineation of the monsoon onset boundaries. In other monsoon regions, there are no clear advantages of increased resolution.

As for the global monsoon onset, we compute the distributions of monsoon withdrawal—the pentad when fractional accumulation first becomes $\geqslant 0.8$—in simulations and observations (Fig. 9). The observed monsoon withdraws from higher latitudes toward the equatorial monsoon regions. In the NH, the earliest withdrawal over the East Asian monsoon is witnessed in pentad 48 in late August; the latest is over the southern edge of the NH monsoon region in pentad 60 in late October. In the SH, the earliest is over South Africa in pentad 14 in mid-March, and the latest over the northern edge of Australia in pentad 30 in late June. The observed monsoon withdrawal patterns are captured well by all the models, but with relatively later withdrawals over the Australian and North American monsoons by two pentads. There are no obvious differences between the low- and high-resolution configurations, or between GPCP and TRMM. These results suggest monsoon withdrawal is less sensitive to resolution than monsoon onset.

To quantitatively identify the improvements from higher resolution, the summer monsoon onset and withdrawal pentads averaged over each regional monsoon are shown in Fig. 10. In observations, TRMM shows (red dots in Fig. 10) that the monsoon onsets (withdraws) in pentad 33 (52) over India,

30.5 (54) over Southeast Asia, 27.5 (49.5) over East Asia, 7 (28.5) over Australia, 32.8 (53.5) over West Africa, 8.2 (27) over South Africa, 32.4 (56) over North America, and 3.2 (27.2) over South America. Compared with TRMM, the onset pentads of all regional monsoons except the Indian monsoon are systematically earlier in GPCP, the lower-resolution observational dataset, with the largest difference of up to two pentads earlier for the West Africa monsoon. However, the monsoon withdrawal dates from TRMM and GPCP are similar, with a maximum difference of 0.5 pentads. The difference between TRMM and GPCP may suggest that resolution has a greater impact on monsoon onset than on withdrawal. For all domains, the model dispersion far exceeds the differences between TRMM and GPCP. Here, we use the onset and withdrawal derived from TRMM as a reference, due to its higher resolution than GPCP. All models show earlier onsets over East Asia, West Africa, South Africa and North America. The results are consistent with Figs. 8 and 9. Specifically, the largest bias is about 4.5 pentads in MRI-AGCM3.2H over East Asia, 4 pentads in GFDL-HiRAM-C180 over West Africa, 2 pentads in GFDL-HiRAM-C360 over South Africa, and 4.5 pentads in GFDL-hIRAM-C360 over North America. Increased resolution consistently delays the onset of monsoon over East Asia and West Africa in all the AGCMs, matching well with the differences between TRMM and GPCP. However, these improvements from high resolution amount to only one pentad at most—far less than the biases of the corresponding low-resolution models ($\leqslant 4.5$ pentads). A consistently slightly advanced onset in the higher-resolution models (1.5 pentads earlier at most over Southeast Asia) relative to their lower-resolution counterparts is shown over Southeast Asia, Australia, South Africa, North America and South America. For the Indian monsoon, both the biases of the lower-resolution configurations and the improvements in the high-resolution configurations differ greatly among the three AGCMs, indicating less sensitivity of the Indian monsoon onset to resolution.

5. Summary and discussion

In this study, the sensitivity of the annual cycle of the global monsoon to resolution is investigated in three AGCMs: MetUM-GA3, MRI-AGCM3 and GFDL-HiRAM. We compare the output from MetUM-GA3 at N216 (90 km) and N512 (40 km), MRI-AGCM3.2H (60 km) and MRI-AGCM3.2S (20 km), and GFDL-HiRAM-C180 (65 km) and GFDL-HiRAM-C360 (32 km). We find consistent and inconsistent responses across the three AGCMs to increasing resolution.

A graphical summary of the model responses to horizontal resolution is presented in Fig. 11. All the low-resolution AGCMs are biased toward higher annual mean precipitation and stronger solstitial and equinoctial asymmetric modes. With increasing resolution, all the AGCMs show consistent improvements in simulating the precipitation and low-level circulation of the annual mean and the first two annual cycle modes, as determined from the PCCs and ETSs, denoted by the red boxes in Fig. 11. Regionally, higher PCCs are found in the three high-resolution AGCMs for precipitation for the annual mean, solstitial mode, and equinoctial asymmetric mode, for all regional monsoons except the Australian and North American monsoons. The inconsistent response to increased resolution across the three AGCMs over the North American and Australian monsoons may be partly due to their small monsoon areas.

We find that improvements in simulating the onset and withdrawal of the summer monsoons are regionally dependent. No consistent response to resolution is found in simulating monsoon withdrawal. Consistent improvement in simulating the onsets of the East Asian, Southeast Asian and West African monsoons is shown across the three AGCMs, by delaying the onset of the East Asian and West African monsoons and advancing that of the Southeast Asian monsoon. A consistently weakened equinoctial asymmetric mode for the East Asian and West African monsoons with increasing resolution is seen across the three models, reducing the wet biases in the transition seasons. Thus, the summer monsoon onset pentad of the two regional monsoons is systematically delayed in all the high-resolution models relative to their low-resolution counterparts. In contrast, the improvements in monsoon onset for the Southeast Asian monsoon constitute a consistent advancement across all three models. Systematic errors and responses to resolution differ greatly across the three AGCMs for the simulated Indian, North American, and SH (Australian, South African, South American) regional monsoons, and the response to resolution differs across the three AGCMs, indicating the dependence of these regions on physical parameterizations. Nevertheless, better representation of the Indian monsoon is shown in all three AGCMs.

Comparing the impact of resolution on the simulated regional monsoon precipitation annual cycle, this study demonstrates the importance of resolution for the East Asian monsoon and West African monsoon, where improved annual cycles are simulated in the three AGCMs. The positive bias of the equinoctial asymmetric mode over the West African monsoon region is caused by overestimated precipitation in spring; in CMIP5 models, this bias has been linked to the representation of African easterly waves (Martin and Thorncroft, 2015, Fig. 6). Both the AMIP and historical simulations of CMIP5 show wet biases over northern Africa in spring; this bias is significantly reduced in high-resolution models. A possible reason is that the finer resolution weakens the excessive African easterly wave activity over northern Africa and thus reduces rainfall (Martin and Thorncroft, 2015). Over the East Asian monsoon region, the summer monsoon rainfall—particularly the mei-yu rainbelt—is underestimated in many contemporary models (Kang, 2004; Huang et al., 2013). Therefore, the simulated contribution of summer rainfall to the annual total is also underestimated, resulting in relatively faster fractional accumulations of precipitation in spring and an earlier onset of the East Asian monsoon. As shown in Yao et al. (2017), as resolution increases,

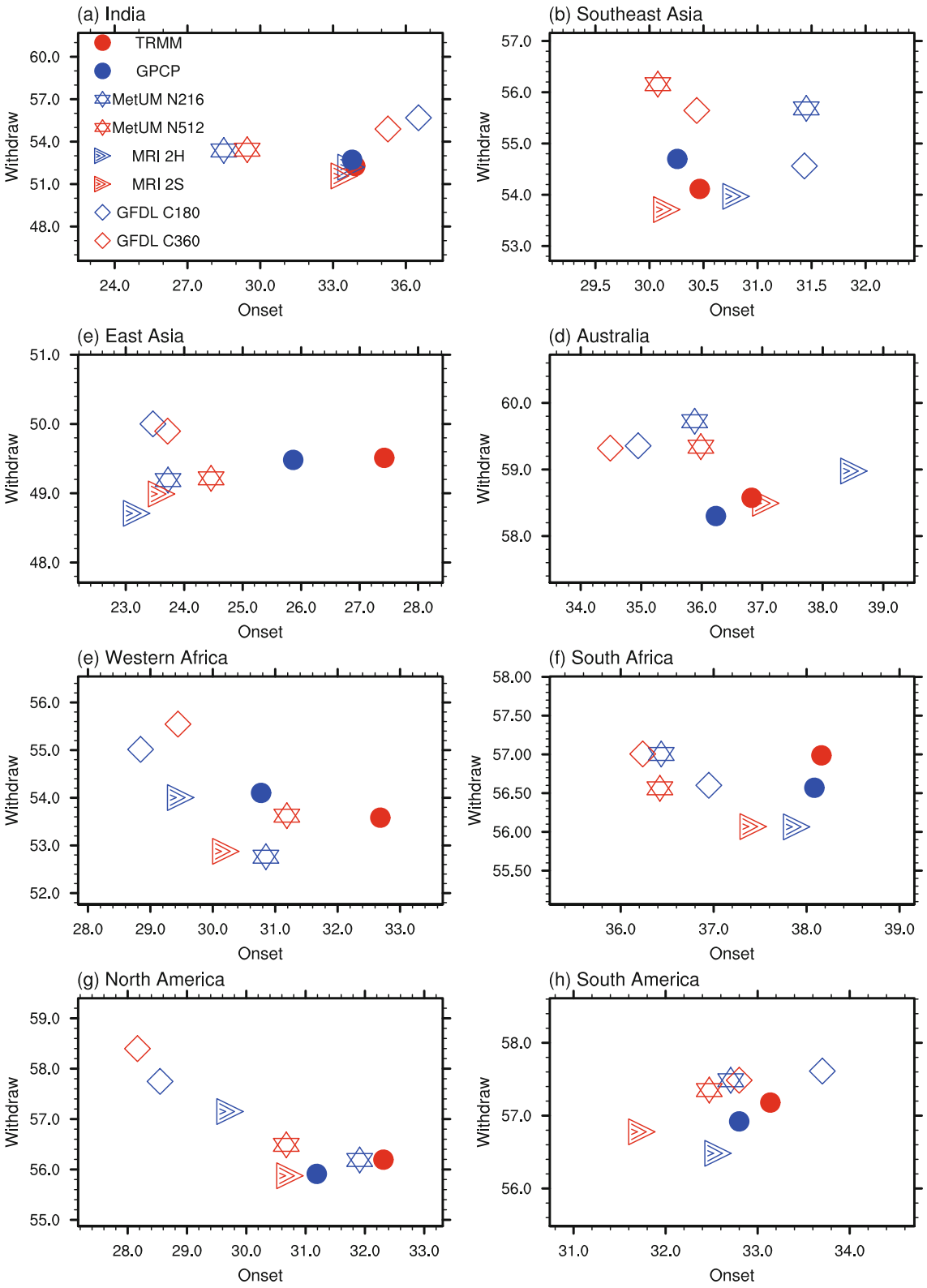

Fig. 10. Monsoon onset (*x*-axis) and withdrawal pentad (*y*-axis) averaged over the (a) Indian, (b) Southeast Asian, (c) East Asian, (d) Australian, (e) West African, (f) South African, (g) North American, and (h) South American monsoons. Note: for SH locations (Australian, South African, and South American monsoons), the pentads were reordered to July–June prior to the analysis. The dots, stars, triangles and diamonds represent the results from the observations, MetUM-GA3, MRI-AGCM3 and GFDL-HiRAM, respectively, with high-resolution configurations in red and low-resolution configurations in blue.

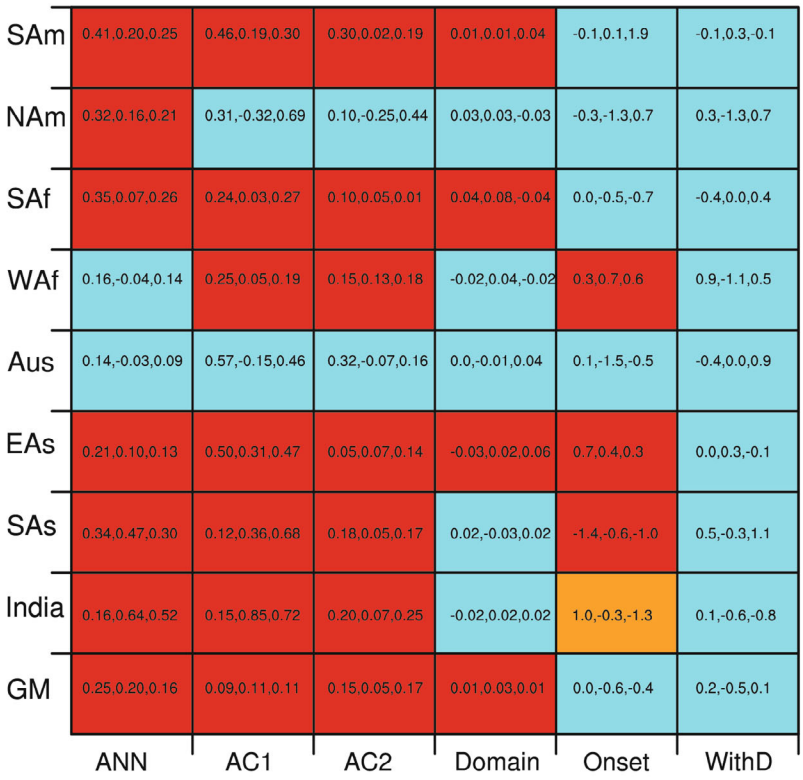

Fig. 11. Improvement in the simulation of the annual cycle of global monsoon precipitation with horizontal resolution. Red boxes indicate high-resolution consistently improves performance across all three AGCMs; blue boxes indicate improvements with resolution are inconsistent; orange boxes indicate a better simulation is shown in all three high-resolution AGCMs but the responses to resolution are inconsistent across models. The values from left to right in each box are the difference between high- and low-resolution configurations of MetUM-GA3, MRI-AGCM3 and GFDL-HiRAM, respectively. The metric for the annual modes, including annual mean (ANN), solstitial mode (AC1), and the equinoctial asymmetric mode (AC2), is the PCC with TRMM. The metrics for the monsoon domain and monsoon onset/withdrawal are the ETS and the onset/withdrawal pentad, respectively.

intensified northerly flow over the central northern areas of China and southerly flow to the south of Japan is found both from the AMIP simulations in CMIP5 and in CAM5 simulations with different resolutions. Those changes with resolution are related to the topography-driven barotropic Rossby waves downstream of the Tibetan Plateau (Yao et al., 2017). However, how the increased resolution affects the regional circulation remains inconclusive and deserves further investigation.

Although several consistent responses to resolution are identified across the three AGCMs considered, large differences still exist, especially over the Indian monsoon region. Large differences in the sensitivity to resolution over the Indian monsoon region are found between MetUM-GA3 and MRI-AGCM3, particularly in synoptic and intraseasonal variability, such as monsoon low-pressure systems (Ogata et al., 2017). Those inconsistencies across models demonstrate the importance of improving physical parameterizations to reduce these systematic errors. This paper highlights the need for further multi-model comparisons to determine the added value of horizontal resolution in climate simulations.

Acknowledgements. This work was jointly supported by the National Natural Science Foundation of China (Grant Nos. 41420104006, 41330423), Program of International S&T Cooperation under grant 2016YFE0102400, and the UK–China Research & Innovation Partnership Fund through the Met Office Climate Science for Service Partnership (CSSP) China as part of the Newton Fund. Nicholas P. KLINGAMAN was funded by an Independent Research Fellowship from the Natural Environment Research Council (Grant No. NE/L010976/1).

REFERENCES

Adler, R. F., and Coauthors, 2003: The version-2 global precipitation climatology project (GPCP) monthly precipitation analysis (1979–present). *Journal of Hydrometeorology*, **4**, 1147–1167, https://doi.org/10.1175/1525-7541(2003)004<1147:TVGPCP>2.0.CO;2.

Berckmans, J., T. Woollings, M.-E. Demory, P.-L. Vidale, and M. Roberts, 2013: Atmospheric blocking in a high resolution climate model: Influences of mean state, orography and eddy forcing. *Atmospheric Science Letters*, **14**, 34–40, https://doi.org/10.1002/asl2.412.

Chen, J. H, and S. J. Lin, 2013: Seasonal predictions of tropical cyclones using a 25-km-resolution general circulation model. *J. Climate*, **26**, 380–398, https://doi.org/10.1175/JCLI-D-12-00061.1.

Demory, M.-E., P. L. Vidale, M. J. Roberts, P. Berrisford, J. Strachan, R. Schiemann, and M. S. Mizielinski, 2014: The role of horizontal resolution in simulating drivers of the global hydrological cycle, *Clim. Dyn.*, **42**(7–8), 2201–2225.

Dong, G. T., H. Zhang, A. Moise, L. Hanson, P. Liang, and H. Ye, 2016: CMIP5 model-simulated onset, duration and intensity of the Asian summer monsoon in current and future climate. *Climate Dyn*., **46**, 355–382, https://doi.org/10.1007/s00382-015-2588-z.

Donlon, C. J., M. Martin, J. Stark, J. Roberts-Jones, E. Fiedler, and W. Wimmer, 2012. The Operational Sea Surface Temperature and Sea Ice Analysis (OSTIA) system. *Remote Sensing of Environment*, **116**, 140–158, https://doi.org/10.1016/j.rse.2010.10.017.

Endo, H., A. Kitoh, T. Ose, R. Mizuta, and S. Kusunoki, 2012: Future changes and uncertainties in Asian precipitation simulated by multiphysics and multi-sea surface temperature ensemble experiments with high-resolution Meteorological Research Institute atmospheric general circulation models (MRI-AGCMs). *J. Geophys. Res*., **117**, D16118, https://doi.org/10.1029/2012JD017874.

Hack, J. J., J. M. Caron, G. Danabasoglu, K. W. Oleson, C. Bitz, and J. E. Truesdale, 2006: CCSM-CAM3 climate simulation sensitivity to changes in horizontal resolution, *J. Climate*, **19(11)**, 2267–2289.

Higgins, R. W., and W. Shi, 2001: Intercomparison of the principal modes of interannual and intraseasonal variability of the North American Monsoon System. *J. Climate*, **14**, 403–417, https://doi.org/10.1175/1520-0442(2001)014<0403:IOTPMO>2.0.CO;2.

Huang, D. Q., J. Zhu, Y.-C. Zhang, and A.-N. Huang, 2013: Uncertainties on the simulated summer precipitation over eastern China from the CMIP5 models. *J. Geophys. Res*., **118**, 9035–9047, https://doi.org/10.1002/jgrd.50695.

Huffman G. J., and Coauthors, 2007: The TRMM multisatellite precipitation analysis (TMPA): Quasi-global, multiyear, combined-sensor precipitation estimates at fine scales. *Journal of Hydrometeorology*, **8**, 38–55, https://doi.org/10.1175/JHM560.1.

Hung, C. W., and M. Yanai, 2004: Factors contributing to the onset of Australian summer monsoon. *Quart. J. Roy. Meteor. Soc*., **130**, 739–758, https://doi.org/10.1256/qj.02.191.

Johnson, S. J., and Coauthors, 2016: The resolution sensitivity of the South Asian monsoon and Indo-Pacific in a global 0. 35° AGCM. *Climate Dyn*., **46**, 807–831, https://doi.org/10.1007/s00382-015-2614-1.

Jolliffe, I. T., and D. B. Stephenson, 2003: *Forecast Verification*: *A Practitioner's Guide in Atmospheric Science*. Wiley, 240 pp.

Kalnay, E., and Coauthors, 1996: The NCEP/NCAR 40-Year Reanalysis Project. *Bull. Amer. Meteor. Soc.*, **77**, 437–472.

Kang, I.-S., 2004: Current status of AGCM monsoon simulations. *East Asian Monsoon*, C.-P. Chang, Ed., World Scientific, 301–331, https://doi.org/10.1142/9789812701411_0008.

Kitoh, A., and S. Kusunoki, 2008: East Asian summer monsoon simulation by a 20-km mesh AGCM. *Climate Dyn*., **31**, 389–401, https://doi.org/10.1007/s00382-007-0285-2.

Krishnamurti, T. N., and Y. Ramanathan, 1982: Sensitivity of the monsoon onset to differential heating. *J. Atmos. Sci*., **39**, 1290–1306, https://doi.org/10.1175/1520-0469(1982)039<1290:SOTMOT>2.0.CO;2.

Kusunoki, S., 2016: Is the global atmospheric model MRI-AGCM3- 2 better than the CMIP5 atmospheric models in simulating precipitation over East Asia? *Climate Dyn*., https://doi.org/10.1007/s00382-016-3335-9. (in Press)

Li, J., R. C. Yu, W. H. Yuan, H. M. Chen, W. Sun, and Y. Zhang., 2015: Precipitation over East Asia simulated by NCAR CAM5 at different horizontal resolutions. *Journal of Advances in Modeling Earth Systems*, **7**, 774–790, https://doi.org/10.1002/2014MS000414.

Li, P. X., T. J. Zhou, and X. L. Chen, 2017: Water vapor transport for spring persistent rains over southeastern China based on five reanalysis datasets. *Climate Dyn*., https://doi.org/10.1007/s00382-017-3680-3. (in Press)

Liu, Y. M., J. C. L. Chan, J. Y. Mao, and G. X. Wu, 2002: The role of Bay of Bengal convection in the onset of the 1998 South China Sea summer monsoon. *Mon. Wea. Rev*., **130**, 2731–2744, https://doi.org/10.1175/1520-0493(2002)130<2731:TROBOB>2.0.CO;2.

Mao, J. Y., and G. X. Wu, 2007: Interannual variability in the onset of the summer monsoon over the eastern Bay of Bengal. *Theor. Appl. Climatol*., **89**, 155–170, https://doi.org/10.1007/s00704-006-0265-1.

Martin, E. R., and C. Thorncroft, 2015: Representation of African easterly waves in CMIP5 models. *J. Climate*, **28**, 7702–7715, https://doi.org/10.1175/JCLI-D-15-0145.1.

Mizielinski, M. S., and Coauthors, 2014: High resolution global climate modelling; the UPSCALE project, a large simulation campaign. *Geoscientific Model Development*, **7**, 563–591, https://doi.org/10.5194/gmdd-7-563-2014.

Mizuta, R., and Coauthors, 2012: Climate simulations using MRI-AGCM3. 2 with 20-km grid. *J. Meteor. Soc. Japan*, **90A**, 233–258, https://doi.org/10.2151/jmsj.2012-A12.

Ogata, T., S. J. Johnson, R. Schiemann, M. E. Demory, R. Mizuta, K. Yoshida, and O. Arakawa, 2017: The resolution sensitivity of the Asian summer monsoon and its inter-model comparison between MRI-AGCM and MetUM. *Climate Dyn*., **49**, 3345–3361, https://doi.org/10.1007/s00382-016-3517-5.

Raia, A., and I. F. A. Cavalcanti, 2008: The life cycle of the South American monsoon system. *J. Climate*, **21**, 6227–6246, https://doi.org/10.1175/2008JCLI2249.1.

Rayner, N. A., D. E. Parker, E. B. Horton, C. K. Folland, L. V. Alexander, D. P. Rowell, E. C. Kent, and A. Kaplan, 2003: Global analyses of sea surface temperature, sea ice, and night marine air temperature since the late nineteenth century. *J. Geophys. Res*., **108**, 4407, https://doi.org/10.1029/2002JD002670.

Roberts, M. J., and Coauthors. 2009: Impact of resolution on the tropical Pacific circulation in a matrix of coupled models, *J.*

Climate, **22(10)**, 2541–2556.

Saha S, and Coauthors, 2010: The NCEP climate forecast system reanalysis. *Bull. Amer. Meteor. Soc.*, **91 (8)**, 1015–1057, https//doi.org/10.1175/2010BAMS3001.1.

Sperber, K. R., and H. Annamalai, 2014: The use of fractional accumulated precipitation for the evaluation of the annual cycle of monsoons. *Climate Dyn*., **43**, 3219–3244, https://doi.org/10.1007/s00382-014-2099-3.

Sperber, K. R., H. Annamalai, I.-S. Kang, A. Kitoh, A. Moise, A. Turner, B. Wang, and T. Zhou, 2013: The Asian summer monsoon: An inter comparison of CMIP5 vs. CMIP3 simulations of the late 20th century. *Climate Dyn*., **41**, 2711–2744, https://doi.org/10.1007/s00382-012-1607-6.

Sultan, B., and S. Janicot, 2003: The West African monsoon dynamics. Part II: The "Preonset" and "Onset" of the summer monsoon. *J. Climate*, **16**, 3407–3427, https://doi.org/10.1175/1520-0442(2003)016<3407:TWAMDP>2.0.CO;2.

Taylor, K. E., R. J. Stouffer, and G. A. Meehl, 2012: An overview of CMIP5 and the experiment design. *Bull. Amer. Meteor. Soc.*, **93**, 485–498, https://doi:org/10.1175/BAMS-D-11-00094.1.

Trenberth, K. E., D. P. Stepaniak, and J. M. Caron. 2000: The global monsoon as seen through the divergent atmospheric circulation. *J. Climate*, **13**, 3 969–3 993, https://doi.org/10.1175/1520-0442(2000)013<3969:TGMAST>2.0.CO;2.

Wang B., and LinHo, 2002: Rainy season of the Asian-Pacific summer monsoon. *J. Climate*, **15**, 386–398, https://doi.org/10.1175/1520-0442%282002%29015<0386%3ARSOTAP>2.0.CO%3B2.

Wang, B., and Q. H. Ding, 2008: Global monsoon: dominant mode of annual variation in the tropics. *Dyn. Atmos. Oceans*, **44**, 165–183, https://doi.org/10.1016/j.dynatmoce.2007.05.002.

Wu, G. X., and Y. S. Zhang, 1998: Tibetan Plateau forcing and the timing of the monsoon onset over South Asia and the South China Sea. *Mon. Wea. Rev*., **126**, 913–927, https://doi.org/10.1175/1520-0493(1998)126<0913:TPFATT>2.0.CO;2.

Wu, G. X., Y. Guan, Y. M. Liu, J. H. Yan, and J. Y. Mao, 2012: Air–sea interaction and formation of the Asian summer monsoon onset vortex over the Bay of Bengal. *Climate Dyn*., **38**, 261–279, https://doi.org/10.1007/s00382-010-0978-9.

Xu, J. J., and J. C. L. Chan, 2001: First transition of the Asian summer monsoon in 1998 and the effect of the Tibet- tropical Indian ocean thermal contrast. *J. Meteor. Soc. Japan*, **79**, 241–253, https://doi.org/10.2151/jmsj.79.241.

Yao, J. C., T. J. Zhou, Z. Guo, X. L. Chen, L. W. Zou, and Y. Sun, 2017: Improved performance of high-resolution atmospheric models in simulating the East Asian summer monsoon rain belt. *J. Climate*, **30**, 8825–8840, https://doi.org/10.1175/JCLI-D-16-0372.1.

Yu, B., and J. M. Wallace, 2000: The principal mode of interannual variability of the North American Monsoon System. *J. Climate*, **13**, 2794–2800, https://doi.org/10.1175/1520-0442(2000)013<2794:TPMOIV>2.0.CO;2.

Zhang L. X., P. L. Wu, T. J. Zhou, M. J. Roberts, and R. Schiemann, 2016: Added value of high resolution models in simulating global precipitation characteristics. *Atmospheric Science Letters*, **17**, 646–657, https://doi.org/10.1002/asl.715.

Zhao, M., I. M. Held, S.-J. Lin, and G. A. Vecchi, 2009: Simulations of global hurricane climatology, interannual variability, and response to global warming using a 50-km resolution GCM. *J. Climate*, **22**, 6653–6678, https://doi.org/10.1175/2009JCLI3049.1.

Zhou, T., D. Y. Gong, J. Li, and B. Li, 2009: Detecting and understanding the multi-decadal variability of the East Asian Summer Monsoon—Recent progress and state of affairs. *Meteorologische Zeitschrift*, **18 (4)**, 455–467, https://doi.org/10.1127/0941-2948/2009/0396.

Zhou, T. J., and Coauthors, 2017: A robustness analysis of CMIP5 models over the East Asia-Western North Pacific Domain. *Engineering*, **3**, 773–778, https://doi.org/10.1016/J.ENG.2017.05.018.

Zou, L. W., and T. J. Zhou, 2015: Asian summer monsoon onset in simulations and CMIP5 projections using four Chinese climate models. *Adv. Atmos. Sci*., **32**, 794–806, https://doi.org/10.1007/s00376-014-4053-z.